Available online at www.sciencedirect.com
SCIENCE DIRECT
Journal of Catalysis 233 (2005) 100–108
JOURNAL OF CATALYSIS
www.elsevier.com/locate/jcat

Observation of a compensation relation for *n*-hexane adsorption in zeolites with different structures: implications for catalytic activity

C.E. Ramachandran [a], B.A. Williams [b], J.A. van Bokhoven [c], J.T. Miller [a,*]

[a] *BP Research Center, 150 W. Warrenville Rd., Naperville, IL 60563, USA*
[b] *Innovene, 150 W. Warrenville Rd., Naperville, IL 60563, USA*
[c] *Institute for Chemical and Bioengineering, Swiss Federal Institute of Technology (ETH) Zurich, 8093, Zurich, Switzerland*

Received 15 February 2005; revised 5 April 2005; accepted 14 April 2005

Available online 23 May 2005

Abstract

The Henry's equilibrium constant and enthalpy of *n*-hexane adsorption at low coverage have been determined at 423 K for zeolites of different structural types that have been subjected to different treatments. The Henry's constant and enthalpy of adsorption increased as the pore size decreased as MFI > MOR > BEA > FAU. Brønsted acid sites and non-framework Al produced through steaming gave smaller increases, and changes due to alkali or lanthanide ions had little effect. From the enthalpy of adsorption and the Henry's equilibrium constant, the entropy of adsorption was calculated. Despite the large differences in structure and composition of the zeolites, there is a linear correlation, or compensation relation, between the entropy and enthalpy of adsorption for all of the zeolites. Combined with previous work in which the same zeolites exhibited a linear kinetic compensation, or Constable relation, for the monomolecular cracking of *n*-hexane, these results support the proposal that the intrinsic acid strengths of active Brønsted acid sites in zeolites of different structures or silica-to-alumina ratios with Lewis acid sites from nonframework Al are similar.

Keywords: Compensation effect; Enthalpy of *n*-hexane adsorption in zeolites; Henry's constant for *n*-hexane on zeolites; Zeolite acidity; Alkane sorption; MFI; Y zeolite; Mordenite; Beta zeolite; Intrinsic zeolite activity

1. Introduction

Zeolites are widely used as solid acid catalysts in industrial petrochemical processes, such as fluid catalytic cracking, hydro-cracking, paraffin isomerization, aromatic alkylation, xylene isomerization, and toluene disproportionation [1]. The structure of zeolites is composed of silicon and aluminum oxide tetrahedra and charge-balancing cations. It is generally accepted that in acidic zeolites, the active site is a proton localized on an oxygen ion, bridging aluminum to silicon. Several studies have shown that the cracking activity increases in direct proportion to the number of Brønsted acid sites [2–4]. In addition, it has been observed that for many acid-catalyzed reactions, the conversion varies significantly for zeolites with differing structures or postsynthesis modifications. From such observations grew the hypothesis that the strength of Brønsted acid sites significantly increases with the Si/Al ratio [5–7]; a decrease in the T–O–T bond angle [8,9]; the presence of Lewis acid, nonframework aluminum [2,10–18], or charge-balancing polyvalent cations [19–21]. For example, although high-temperature steaming of zeolites leads to the loss of structural aluminum and a decrease in the number of Brønsted acid sites, nonframework Al generates Lewis acid sites and increases catalytic activity. One proposal suggests that Lewis acid sites withdrew electron density from the Brønsted sites, leading to catalytic sites with enhanced acid strength [18,22,23]. If Brønsted sites with enhanced acid strength were present, the intrinsic kinetic parameters, that is, the rate constant and activation energy, would be significantly different from those of nonmodified Brønsted acid sites.

* Corresponding author.
E-mail address: millejt1@bp.com (J.T. Miller).

0021-9517/$ – see front matter © 2005 Published by Elsevier Inc.
doi:10.1016/j.jcat.2005.04.017

Paraffin cracking is a model reaction that is often used to characterize the strength of Brønsted acid sites in zeolites. Depending upon the reaction conditions, there are two reaction pathways for paraffin cracking, monomolecular and bimolecular [24–26]. Under conditions where monomolecular alkane cracking dominates, studies have shown that alkane adsorption contributes to the apparent kinetics [27–29]. Several studies have successfully interpreted the differences in apparent rates as being due mainly to the differences in heats of adsorption and the alkane surface coverage [27–34]. For example, in H-MFI, the cracking rate increased and the apparent activation energy decreased with increased length of the alkane [27,29]. It was suggested that for larger *n*-alkanes the increased heat of adsorption leads to a higher surface coverage and, thus, an increased cracking rate. After correcting for the adsorption enthalpy, the intrinsic activation energies for all *n*-alkanes were shown to be identical. Similar observations have been made for hydro-isomerization over Pt zeolites [35,36].

For cracking of *n*-alkanes on H-MFI, there was also a linear correlation between the apparent activation energy and the logarithm of the apparent pre-exponential factor [28, 34]. This is also referred to as a kinetic compensation effect or a Constable relation. A Constable relation was also observed for monomolecular cracking of *n*-hexane for zeolites of different structures and postsynthesis treatments [28]. The implication of the later study was that the intrinsic kinetic parameters of the different zeolites are very similar, contrary to the earlier proposal for zeolites with enhanced acid strength. The linear Constable correlation also implies there is a linear compensation relation between the entropy and enthalpy of adsorption.

In this study, the Henry's equilibrium constant and enthalpy of *n*-hexane adsorption at low surface coverage have been determined for zeolites of different structures and postsynthesis treatments. In addition, the entropy of adsorption has been calculated and is shown to be linearly proportional to the enthalpy of adsorption. These results support the proposal that the differences in monomolecular *n*-paraffin cracking conversion with different zeolites are due primarily to changes in the adsorption properties and that the intrinsic acid strengths of the active Brønsted sites are similar.

2. Experimental

Zeolite samples used for this study are listed in Table 1. Na-Y (LZY-54 from UOP), H-USY (LZY-84 from UOP), H-BEA (from Engelhard), H-MOR (LZM-8 from Union Carbide), Na-MOR (LZM-5 from Union Carbide), and H-MFI (CBV-8020 from Zeolyst) were commercial samples and were calcined in flowing air for 5 h at 725 K. Silicalite was synthesized in our laboratory as follows: in 510 g H_2O, 16.3 g NaOH, 32.5 g tetrapropylammonium bromide, 452 g Nalco 2327 silica sol (40% in H_2O), and 10.6 g H_2SO_4 were mixed to give a pH of 12.3. The slurry was placed in a Teflon-lined autoclave and stirred at 250 rpm at 440 K for 24 h. The yield of silicalite was 99%. The crystallinity was 95% (determined by XRD) with single crystals (no apparent amorphous material) of $8 \times 7 \times 5$ μm size, determined by SEM. Na-Y was partially La^{3+} ion-exchanged by the addition of 11.7 g $La(NO_3)_3 \cdot 6H_2O$ to 75 g NaY (LZY-54) in 300 ml H_2O. The slurry was heated and stirred at 350 K for 2 h, filtered, washed twice in 200 ml H_2O, dried, and calcined at 575 K for 3 h. The La-Y zeolite was subsequently exchanged with 75 g NH_4NO_3 in 300 ml H_2O at 350 K for 1 h, filtered, washed twice in 200 ml H_2O, dried, and calcined at 725 K for 3 h. H-MFI was partially Cs^+ ion-exchanged by the addition of 1.08 g $CsNO_3$ to 20 g of H-MFI (CBV 8020) in 100 ml H_2O. The slurry was heated and stirred at 350 K for 1 h, filtered, washed twice with 200 ml cold H_2O, dried at 375 K, and calcined at 575 K for 5 h. Elemental analysis was determined by ICP, and the N_2 BET micropore volume and surface area were determined with a Micromeritics ASAP 2400 at liquid-nitrogen temperature. The results are given in Table 1.

A schematic of the adsorption and microcalorimeter apparatus is shown in Fig. 1a. All tubing used for the apparatus was stainless steel. A calorimeter block, two exchangeable pressure transducers, and a dosing loop were enclosed in an insulated convection oven, which was maintained at 423 K.

Table 1
Zeolite micropore volumes and chemical compositions

Sample	Unit cell composition	XRD/ICP unit cell		N_2 BET micropore volume (cc/g)	Composition (wt%)
		Volume (cc/g)	Void volume[a] (cc/g)		
H-USY	$H_{26}Al_{26}Si_{166}O_{384}$	0.79	0.62	0.26	Al = 11.1; Na = 0.1
H,La-Y	$H_{25}Na_{11}La_6Al_{54}Si_{138}O_{384}$	0.72	0.55	0.26	Al = 11.3; La = 6.5; Na = 2.1
Na-Y	$Na_{54}Al_{54}Si_{138}O_{384}$	0.71	0.53	0.32	Na = 10.1; Al = 11.5
H-BEA	$H_4Al_4Si_{60}O_{128}$	0.67	0.47	0.17	Al = 2.8
Na-MOR	$Na_6Al_6Si_{42}O_{96}$	0.67	0.48	0.14	Na = 4.9; Al = 5.7
H-MOR	$H_3Al_3Si_{45}O_{96}$	0.69	0.49	0.18	Al = 3.3
Silicalite	$Si_{96}O_{192}$	0.55	0.35	0.10	Al < 0.01
H,Cs-MFI	$Cs_{0.7}H_{1.3}Al_2Si_{94}O_{192}$	0.55	0.35	0.12	Cs = 1.7; Al = 1.0
H-MFI	$H_2Al_2Si_{94}O_{192}$	0.56	0.36	0.10	Al = 1.0

[a] The volume of ions was subtracted from the total unit cell volume.

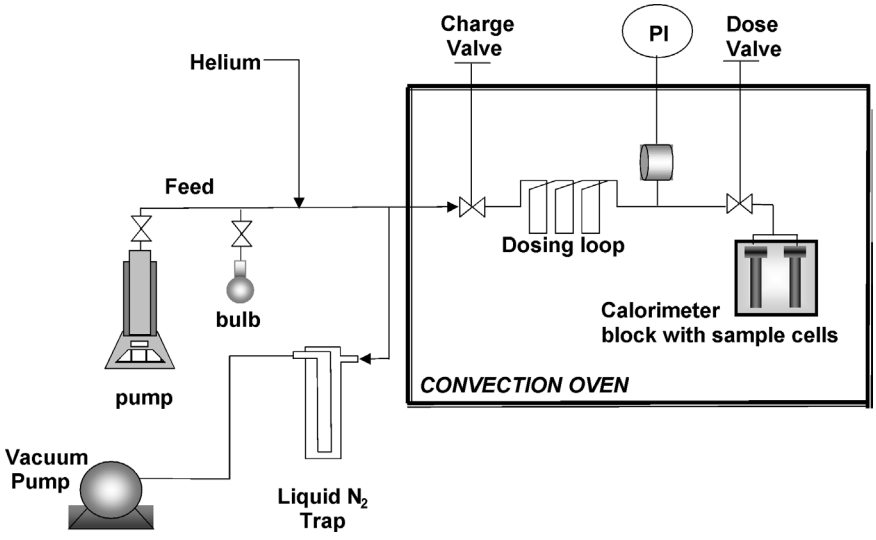

(a)

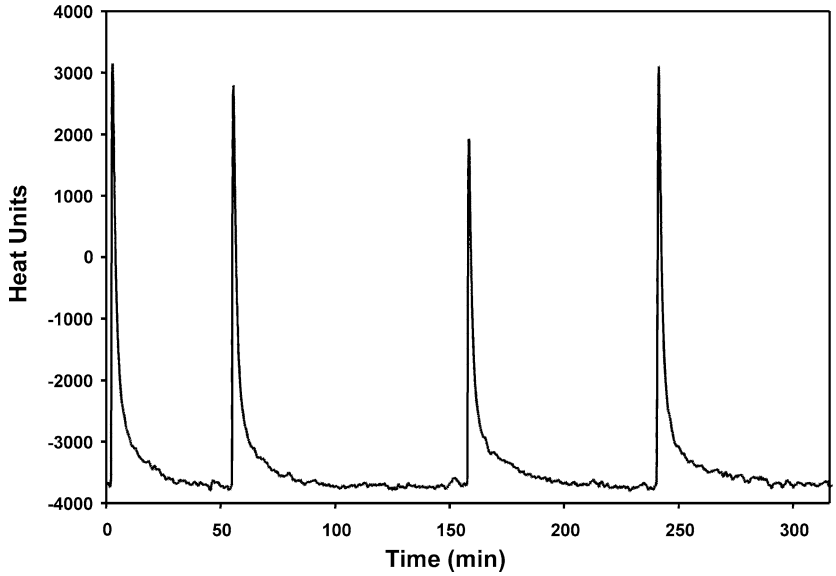

(b)

Fig. 1. (a) Schematic diagram of the microcalorimetry apparatus. (b) Experimental calorimetry data of heat evolved during four sequential additions of *n*-hexane on H-MFI at 423 K.

The pressure transducers (MKS Instruments model 616A) used were in the range of 0–10 and 0–10,000 Torr for the calorimetry and isotherm measurements, respectively. Both were bakeable up to 673 K and were calibrated at 423 K, with a reading error of ±0.1%. The charge and dose valves used to separate the dosing loop from the feed lines and the calorimeter cells, respectively, were manually operated Hoke (4235N6Y) and Swagelok (SS-4UG-V51) stainless-steel valves. The calorimeter was constructed in-house and consisted of two identical stainless-steel chambers enclosed in an aluminum block, attached to the system via flanges fitted with copper gaskets. One chamber served as a reference cell and the other as the catalyst sample cell. Heat flux transducers surrounded the two calorimeter cells and produced a voltage signal proportional to heat flow. The integral of the voltage difference between sample and reference during an adsorbate dose was then proportional to the heat of adsorption. A Welch Duo Seal rough vacuum pump and a liquid nitrogen trap were used to establish vacuum conditions over the whole system with baseline pressures on the order of 10^{-2} Torr.

Volumes for the dosing loop and sample cells were calculated based on helium expansion into a known volume chamber and a blind flange in place of the calorimeter. The volumes were obtained from averaging over at least five different doses of helium, yielding an error of less than 2%.

We calibrated the calorimetry unit by inserting a miniature cartridge heater into the calorimeter sample chamber, which was filled to the normal loading level with α-alumina particles. A previously calibrated power meter monitored the

total electrical (heat) energy supplied to the calorimetry cell. Calibration consisted of applying known amounts of power over a specific period of time and then determining the heat response peak areas by integrating from the baseline in the calorimeter heat trace. Ample time was allowed between heat inputs for the re-establishment of the baseline. The resultant calibration plot was exactly linear and encompassed the entire range of operation for adsorption experiments, ensuring that all experimental measurements lay within the linear regime of the detector.

The adsorbate used for this study was *n*-hexane (99.8% purity) from Sigma-Aldrich. A separate, larger sample chamber within the oven was used for high coverage isotherms. Before an adsorption experiment, 10 g calcined catalyst was evacuated at less than 10^{-2} Torr at 423 K for 15 h. The void volume of the sample chamber was determined by helium expansion. Subsequently, the helium gas was evacuated before the start of *n*-hexane adsorption. *n*-Hexane was delivered to the system via a dosing loop by an Isco 500D syringe pump or as vapor from a liquid bulb (Fig. 1a). Before delivery as a vapor, the *n*-hexane was purified by three freeze–pump–thaw cycles to remove dissolved gasses.

Similar procedures were used for the calorimetry experiments, except that the calorimeter block and its two sample chambers were attached to the adsorption system containing ca. 500 mg of sample. During the calorimetry experiment, the dosing and adsorption pressures, as well as the heat evolved, were determined. When the system reached thermal equilibrium, as indicated by the return to thermal baseline, the next dose was administered. With dose sizes of 5 µmol, the heat released was between 0.2 and 3.5 J. A typical calorimetry data plot is shown in Fig. 1b. The signal-to-noise ratio was about 60, and the error for the heat of adsorption was 2%, based on the repeatability with silicalite.

3. Results

The micropore volumes of the zeolites were determined by saturation of N_2 adsorption at liquid-nitrogen temperature. The pore volume decreases in the order Na-Y > H-USY, H,La-Y > H-MOR, H-BEA > Na-MOR > silicalite, H-MFI, H,Cs-MFI. Generally, the pore volume decreases with decreasing pore size. Steaming to produce H-USY results in dealumination, partial loss of crystallinity, and smaller pore volume. The amount of framework Al was determined from the XRD unit cell volume [37]. Dealuminated H-MOR, however, increases the available pore volume compared with Na-MOR, and incorporation of Al into silicalite or ion exchange of H^+ by Cs^+ in MFI has little effect on the pore volume.

Fig. 2 shows the characteristic Type I isotherm for *n*-hexane at 423 K for H-MFI. In the low coverage, or Henry's law region (up to about 100 Torr), the coverage increases linearly with pressure. At pressures higher than about 2500 Torr, the pores are saturated with hexane molecules. For this study, adsorption capacity and enthalpy were determined in the Henry's regime, since the *n*-hexane surface coverage is very low at the temperatures and pressures typical of monomolecular cracking. Fig. 3 shows typical low coverage adsorption isotherms (up to about 0.2 Torr) for several zeolites. For the sake of clarity, only six samples are shown. The amount adsorbed at low pressure decreases in the order H-MOR > silicalite, H-MFI, H,Cs-MFI > H-BEA > Na-MOR > Na-Y > H,La-Y > H-USY. This order is almost opposite that determined for saturation coverage; that is, the smaller the pore size, the higher the coverage. H-MOR is the exception to this general trend, since the dealumination gives an increase in adsorption capacity at low and saturation coverage.

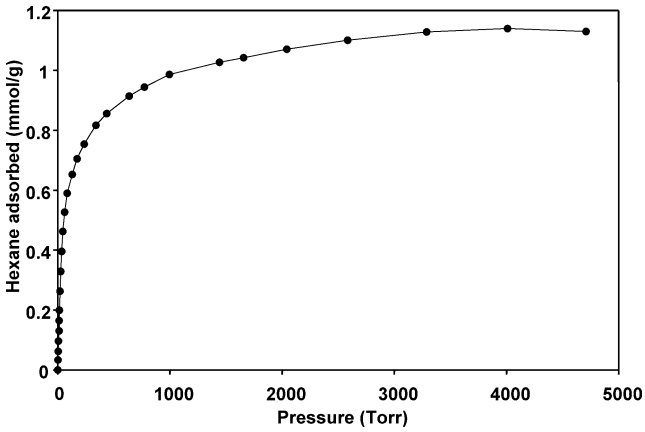

Fig. 2. *n*-Hexane adsorption isotherm for H-MFI at 423 K.

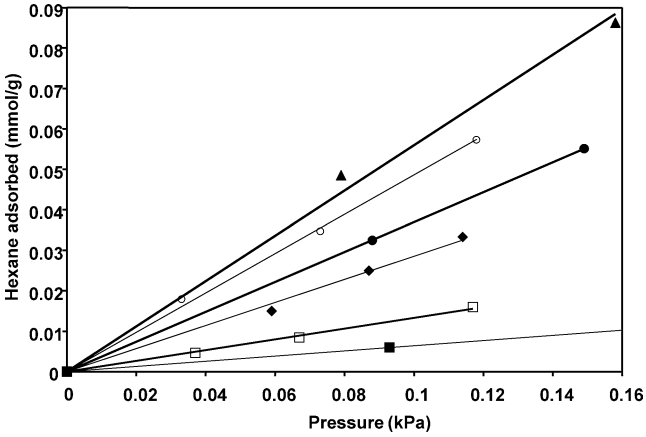

Fig. 3. Low coverage isotherms for *n*-hexane in various zeolites at 423 K. H-MOR (▲), Silicalite (●), H,Cs-MFI (○), H-BEA (◆), Na-Y (□), and H,La-Y (■).

The dimensionless adsorption constant, K_{ads}, was calculated from the experimental adsorption constant, K_{exp}, using Eq. (1), where R is the gas constant, T is the temperature, and V_{ads} is the adsorbent pore volume:

$$K_{ads} = K_{exp} RT / V_{ads}. \quad (1)$$

A linear fit of each adsorption isotherm in Fig. 3 was used for calculation of the Henry's constant, K_{exp}. A more ac-

Table 2
Henry's constants for n-hexane adsorption at 423 K

Sample	Experimental K_{exp} (mmol/g/Torr)	Dimensionless K_{ads} (N_2 pore volume)	Dimensionless K_{ads} (unit cell void volume and composition)
H-USY	0.058	5.85×10^3	2.45×10^3
H,La-Y	0.086	8.75×10^3	4.13×10^3
Na-Y	0.138	1.14×10^4	6.86×10^3
H-BEA	0.337	5.23×10^4	1.89×10^4
Na-MOR	0.297	5.60×10^4	1.63×10^4
H-MOR	0.560	8.20×10^4	3.01×10^4
Silicalite	0.377	1.06×10^5	2.84×10^4
H,Cs-MFI	0.487	1.07×10^5	3.67×10^4
H-MFI	0.416	1.10×10^5	3.04×10^4

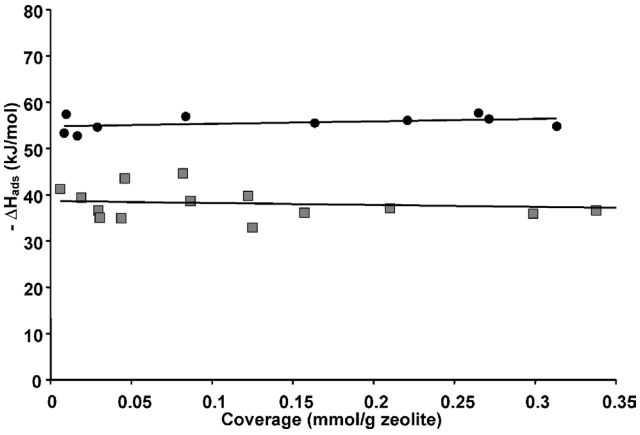

Fig. 4. Heat of adsorption as a function of coverage for n-hexane in H-USY (▩) and H-MFI (●) at 423 K.

curate value of K_{ads} would be based on the n-hexane pore volume, rather than N_2 adsorption, since nitrogen may be adsorbed in regions where n-hexane cannot [38]. However, since the n-hexane pore volume was not obtained, we also calculated K_{ads} by using the XRD unit cell volume from the International Zeolite Association [39] and then subtracting the volume of Si^{+4}, Al^{+3}, O^{-2}, and various cations based on the zeolite composition, determined experimentally by ICP. Table 1 lists the pore volumes from the two methods and Table 2 lists the corresponding equilibrium constants.

Fig. 4 shows the heat of adsorption with increasing coverage for H-USY (from 0.3 to 4 Torr) and for H-MFI (from 0.3 to 1.1 Torr). The $-\Delta H_{ads}$ of H-MFI is greater than that for H-USY. However, both samples displayed an essentially constant heat of adsorption with increasing coverage over this range. The average heat of adsorption calculated from at least the first five adsorption points are listed in Table 3. The value of $-\Delta H_{ads}$ for silicalite, commonly used as a standard, is on the lower end of the range typically reported in the literature [40]. The trends observed between samples are consistent with the literature, and $-\Delta H_{ads}$ decreases in the order H-MFI > Na-MOR > H-MOR, silicalite > H,Cs-MFI > H-BEA > H-USY > H,LaY, Na-Y. The trend appears to be dependent mainly on pore size, with $-\Delta H_{ads}$ decreasing as pore size increases: H-MFI > H-MOR > H-BEA >

Table 3
Enthalpies and entropies of n-hexane adsorption at 423 K

Sample	$-\Delta H_{ads}$ (kJ/mol)	$-\Delta S_{ads}$ (N_2 pore volume) (J/(mol K))	$-\Delta S_{ads}$ (unit cell void volume and composition) (J/(mol K))
H-USY	38.0	17.8	25.1
H,La-Y	33.3	3.3	9.6
Na-Y	33.5	1.5	5.7
H-BEA	47.4	21.8	30.2
Na-MOR	54.7	38.5	48.8
H-MOR	51.6	27.8	36.2
Silicalite	51.4	25.9	36.3
H,Cs-MFI	49.4	20.4	29.4
H-MFI	55.5	34.8	45.4

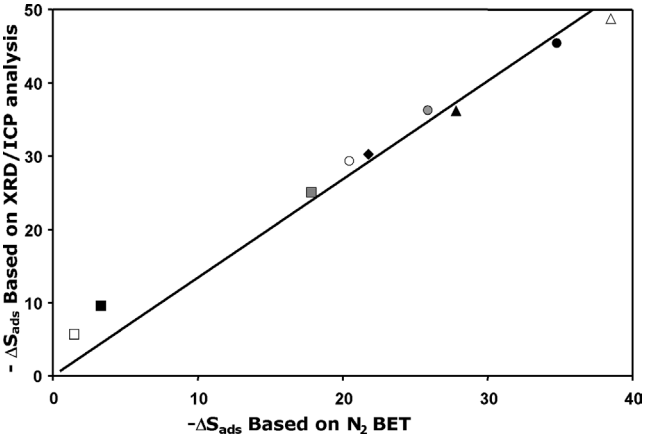

Fig. 5. Linear correlation between $-\Delta S_{ads}$ calculated based on the experimentally determined N_2 micropore volume analysis and XRD unit cell volume with ICP analysis. Na-Y (□), H,La-Y (■), H-USY (▩), H-BEA (◆), H,Cs-MFI (○), Silicalite (◍), H-MFI (●), Na-MOR (△), and H-MOR (▲).

H-USY. Brønsted acid sites also increase $-\Delta H_{ads}$ slightly; for example, $-\Delta H_{ads}$ for H-MFI is higher than that for silicalite. Likewise, $-\Delta H_{ads}$ for H-USY is higher than that of H,La-Y, indicating nonframework aluminum also increases the heat of adsorption.

From the equilibrium constant and the enthalpy of adsorption, the entropy of adsorption was calculated:

$$\Delta G_{ads} = \Delta H_{ads} - T\Delta S_{ads} = -RT\ln(K_{ads}). \quad (2)$$

The entropies of adsorption based on the N_2 micropore volumes and separately from XRD unit cell volumes and ICP are given in Table 3. Fig. 5 shows that the $-\Delta S_{ads}$ calculated by the two methods are consistent with each other. For acidic zeolites, the decrease in $-\Delta S_{ads}$ follows the decrease in pore volume, for example, H-MFI > H-MOR > H-BEA > H-USY. In addition, a comparison of H-MFI with silicalite or H,Cs-MFI demonstrates that Brønsted acid sites also lead to a larger entropy loss upon adsorption.

Fig. 6 is a plot of the enthalpy of adsorption versus entropy of adsorption and clearly shows a linear compensation relation between the two variables. As the $-\Delta H_{ads}$ increases, there is a corresponding increase in $-\Delta S_{ads}$. This

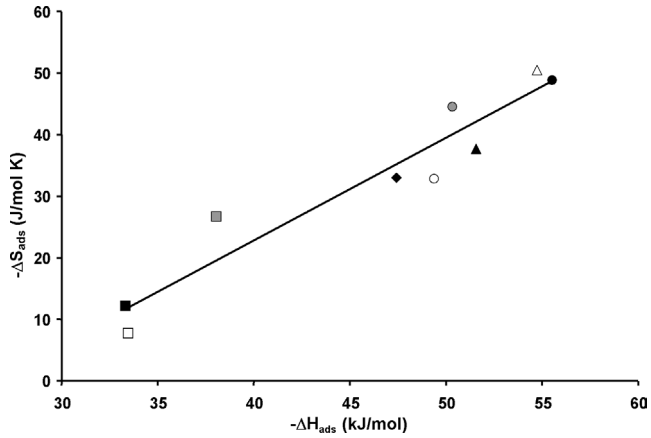

Fig. 6. Enthalpy versus entropy of *n*-hexane adsorption (based on the XRD unit cell volume and ICP elemental analysis) for various zeolites at 423 K. Values were determined from experimental N_2 BET pore volume analysis. Na-Y (□), H,La-Y (■), H-USY (▩), H-BEA (◆), H,Cs-MFI (○), Silicalite (◍), H-MFI (●), Na-MOR (△), and H-MOR (▲).

correlation applies to both the N_2 adsorption and XRD/ICP-based $-\Delta S_{ads}$, since the two quantities are also linearly correlated (Fig. 5). Thus, despite the differences in framework structure, silica-to-alumina ratio, number of Brønsted acid sites, nonframework (Lewis acid) Al or type of cations in the various zeolites, the entropies and enthalpies of adsorption follow a single correlation for *n*-hexane.

4. Discussion

The adsorption compensation relation between $-\Delta S_{ads}$ and $-\Delta H_{ads}$ in Fig. 6 has significant implications for monomolecular cracking by zeolites.

4.1. Monomolecular cracking kinetics

Under conditions where monomolecular alkane cracking dominates (e.g., high temperature, low hydrocarbon pressure, and low conversion), physical adsorption of the alkane reactant contributes to the apparent kinetics [26,27,29], and a Langmuir–Hinshelwood model adequately describes the kinetics [41]. In this model, the main elementary steps can be described as follows:

$$C_6H_{14}(\text{gas}) \Leftrightarrow C_6H_{14}(\text{ads}), \tag{3}$$

$$C_6H_{14}(\text{ads}) + H^+{-}^-OZ \Rightarrow [C_6H_{15}{}^+{-}^-OZ]^{\pm} \Rightarrow \text{cracked products}. \tag{4}$$

Hexane is rapidly adsorbed to equilibrium coverage in the zeolite (Eq. (3)). Adsorbed hexane reacts with a Brønsted site, $H^+{-}^-OZ$, to form a transition state species, $[C_6H_{15}{}^+{-}^-OZ]^{\pm}$, which dissociates to the cracked products (Eq. (4)). Assuming that the kinetic step in Eq. (4) is rate limiting, the apparent reaction rate, r_{app}, can be expressed as follows:

$$r_{app} = k_{int} C_{ads}, \tag{5}$$

where k_{int} and C_{ads} are the intrinsic rate constant and the adsorbed phase reactant concentration, respectively. Under typical monomolecular cracking conditions, the surface coverage of alkane is low, so the denominator of the Langmuir–Hinshelwood expression approaches unity. Application of Henry's law gives

$$r_{app} = k_{int} K_{ads} C_{gas}, \tag{6}$$

where K_{ads} is the dimensionless equilibrium constant and C_{gas} is the concentration of reactant in the gas phase. The rate expression, therefore, is first-order in the reactant partial pressure, and by inspection of Eqs. (5) and (6), the apparent rate constant (k_{app}) is the product of k_{int} and K_{ads}.

4.2. Compensation relations

The temperature dependence of the apparent and intrinsic rate constants is given by the Arrhenius relation, where A_{app} and A_{int} are the apparent and intrinsic pre-exponential factors and E_{app} and E_{int} are the apparent and intrinsic activation energies:

$$k_{app} = A_{app} \exp\left(-\frac{E_{app}}{RT}\right), \tag{7}$$

$$k_{int} = A_{int} \exp\left(-\frac{E_{int}}{RT}\right). \tag{8}$$

The temperature dependency of K_{ads} is

$$K_{ads} = \exp\left(-\frac{\Delta G_{ads}}{RT}\right) = \exp\left(-\frac{\Delta H_{ads}}{RT}\right)\exp\left(\frac{\Delta S_{ads}}{R}\right). \tag{9}$$

Using $k_{app} = k_{int} K_{ads}$, substituting in Eqs. (7)–(9), and separating the enthalpic and entropic terms yields the following relations:

$$E_{app} = E_{int} + \Delta H_{ads}, \tag{10}$$

$$\ln A_{app} = \ln A_{int} + \frac{\Delta S_{ads}}{R}. \tag{11}$$

The (kinetic) Constable correlation, therefore, is the linear dependence between $\ln(A_{app})$ and E_{app}. Both E_{app} ($E_{int} + \Delta H_{ads}$) and A_{app} ($\ln(A_{int}) + \Delta S_{ads}/R$) have contributions from adsorption and kinetics. There are three ways that one can observe a linear Constable relation. First, the differences in apparent activation energy (kinetic contribution) are determined entirely by the differences in adsorption thermodynamics, where there is a linear adsorption compensation relation between $-\Delta H_{ads}$ and $-\Delta S_{ads}$ with substantially constant E_{int} and $\ln(A_{int})$. Second, the adsorption parameters are identical for the catalysts, and there is a linear correlation between E_{int} and $\ln(A_{int})$. The results of this study (e.g., Fig. 6) and others have clearly shown that the adsorption parameters are not constant for different zeolites; thus this possibility will no longer be considered. A final possibility is

that the intrinsic kinetic and adsorption parameters are each linearly related, resulting in the observed Constable relation. The two remaining possibilities will be distinguished below.

4.3. Linear alkanes on H-MFI

The Brønsted acid sites in MFI are generally considered to be chemically equivalent because they are isolated from one another, and, in the absence of diffusion limitations, the activity per site is constant [4]. For the monomolecular cracking of n-alkanes of increasing molecular weight on H-MFI, several studies have successfully interpreted the differences in apparent rates as being due to the differences in reactant $-\Delta H_{ads}$ and thus, surface coverage of alkane. For example, the cracking rate increases and the apparent activation energy decreases as the molecular weight increases. It was suggested that for longer n-alkanes, the increased heat of adsorption leads to a higher surface coverage, resulting in an increased apparent reaction rate. On H-MFI, after correcting for the hexane $-\Delta H_{ads}$, the E_{int} was shown to be identical for all n-alkanes [27,29,33].

For monomolecular n-alkane cracking, MFI also displays a linear Constable relation [29,42]. Since the same MFI catalyst is used, E_{int} and $\ln(A_{int})$ are unchanged and the linear Constable relation results from a linear (adsorption) compensation for n-alkanes. This is an example of the first explanation for the linear Constable correlation presented in Section 4.2 above.

4.4. n-Hexane on different zeolites

A few studies have compared monomolecular cracking over different zeolites, including MFI, MOR, FAU, and BEA [28,30,43]. The present study complements this previous work and shows that evaluation of adsorption is essential to understanding monomolecular cracking activity. In the previous studies, there is disagreement with respect to whether E_{int} is significantly different for different zeolites [30,43]. This discrepancy is discussed in Section 4.4.1, and the relation between the observed kinetic and adsorption compensations is discussed in Section 4.4.2.

4.4.1. Comparison of Babitz et al. [30] and Kotrel et al. [43]

Babitz et al. reported monomolecular n-hexane cracking activity, product selectivity, and activation energies from 753 to 813 K. At the limit of zero conversion, constant product selectivities were observed for H-MFI, H-USY, and H-MOR. Typical n-hexane $-\Delta H_{ads}$ values from the literature were used to obtain E_{int}, via Eq. (10). The main conclusion was that E_{int} values for all zeolites were similar within the accuracy of the data [30]. The uncertainties, however, were large because of the large variations in the enthalpies of adsorption reported in the literature. Kotrel et al. conducted a similar study for H-MFI, H-USY, and H-BEA. In addition to determining selectivities and apparent activation energies, they also determined the heats of adsorption. Whereas USY and BEA had similar intrinsic activation energies, that of MFI was significantly different. In addition, comparison of k_{int} at 623 K indicated that MFI was the more active per acid site, even after correcting for adsorption [43].

Table 4
Comparison of monomolecular n-hexane cracking selectivities and activation energies reported by Babitz et al. [30] and Kotrel et al. [43]

	Babitz et al. [30]			Kotrel et al. [43]		
	H-MFI	H-USY	H-MOR	H-MFI	Dealuminated Y	H-BEA
E_{app} (kJ/mol)	149	177	157	108	114	93
Selectivity (mol%)						
Methane	4	6	5	3	3	0
Ethane	13	11	13	16	9	4
Propane	12	10	11	17	22	36
Propene	30	29	33	32	39	45
Butene	17	12	16	9	16	4

Table 4 shows a comparison of activation energies and product selectivities reported for the two studies. The product selectivities of Babitz et al. are very similar to those reported for n-hexane monomolecular cracking [27,30], whereas those of Kotrel et al. are lower in methane and higher propane, propene, and butene production, suggesting a significant contribution from bimolecular cracking [24]. In addition, the different selectivities indicate a different contribution to the rate from bimolecular cracking for each catalyst. Previously, it was shown that with the transition of monomolecular to bimolecular cracking there is a decrease in the activation energy [44], which is consistent with the lower activation energies for both MFI and USY found by Kotrel.

This interpretation suggests that although the approach of Kotrel et al. was correct and even preferable to that of Babitz et al., the product selectivities of Kotrel et al. indicate a significant contribution from bimolecular cracking, which leads to an inaccurate determination of the monomolecular cracking rates and intrinsic activation energies.

4.4.2. Adsorption and kinetic compensation

For a larger set of zeolites that included H,Na-USY, steamed H-MFI, steamed H-MOR, and a variety of H-MFI catalysts, monomolecular cracking of n-hexane showed a linear Constable correlation, or a kinetic compensation, between E_{app} and $\ln(A_{app})$ [28]. Unlike the Constable correlation observed with n-alkanes on MFI, for these different zeolites there is no implicit reason that the intrinsic kinetic parameters should be identical. In fact, based upon different observed conversions, most studies conclude that the acid strength, and thus the intrinsic kinetic parameters, of different zeolites are significantly different. The prediction from the Constable relation was that there would be a linear adsorption compensation for these zeolites, as observed in Fig. 6 of this study. Apparently, changing the zeolite structure, or modifying a structure by steam or ion-exchange,

gives rise to changes in the heats of adsorption and surface coverage.

The linear Constable plot also implies that the acid strengths of the catalytic sites are very similar [28]. The slope of the Constable plot was ca. 1.1×10^{-3} 1/K, and the slope of the compensation plot was 1.3×10^{-3} 1/K. Within the accuracy of the measurements, these slopes are identical and suggest that the adsorption contribution alone accounts for the majority of the observed kinetic compensation. As in the case of *n*-alkanes on MFI, there is no need to invoke compensation between E_{int} and $\ln(A_{\text{int}})$. That is, E_{int} and $\ln(A_{\text{int}})$ could vary between the zeolites, but only by a small amount with respect to monomolecular cracking. Considering that monomolecular cracking is one of the most demanding acid-catalyzed reactions, this further implies that the intrinsic acid strengths of different zeolites and zeolites subjected to different treatments must be much more similar than previously thought.

5. Conclusion

With the use of microcalorimetry, the enthalpy and entropy of adsorption were determined for zeolites varying in framework structure and treatment. It was observed that $-\Delta H_{\text{ads}}$ increased as pore size decreased. $-\Delta H_{\text{ads}}$ also increased slightly with the presence of Brønsted acid sites and nonframework aluminum. An increase in $-\Delta H_{\text{ads}}$ is indicative of increased surface coverage, resulting in an increase in the number of molecules available for reaction. A common linear compensation relation was observed between $-\Delta H_{\text{ads}}$ and $-\Delta S_{\text{ads}}$. Within the accuracy of the measurements, our results suggest that the adsorption contribution alone accounts for the majority of the previously observed (kinetic) Constable relation for monomolecular *n*-hexane cracking. In addition, our results suggest that the intrinsic acid strengths of the active sites for monomolecular cracking are similar and that the large differences in apparent rate are due primarily to differences in adsorption properties.

Acknowledgments

The authors thank Professor Harold H. Kung for the use of the calorimetry equipment. Joe Scaletta is acknowledged for his assistance in calibration of the calorimeter, and a special thanks to John Juarez for helping us obtain the adsorption isotherms and heats of adsorption.

References

[1] T. Sie, in: H. Van Bekkum, P.A. Jacobs, E.M. Flanigen, J.C. Jansen (Eds.), Introduction to Zeolite Science and Practice, Elsevier, Amsterdam, 2001.
[2] R.A. Beyerlein, G.B. McVicker, L.N. Yacullo, J.J. Ziemiak, J. Phys. Chem. 92 (1988) 1967.
[3] D.H. Olson, W.O. Haag, R.M. Lago, J. Catal. 61 (1980) 390.
[4] W.O. Haag, R.M. Lago, P.B. Weisz, Nature 309 (1984) 589.
[5] D. Barthomeuf, Mater. Chem. Phys. 17 (1987) 49.
[6] E. Dempsey, J. Catal. 33 (1974) 497.
[7] E. Dempsey, J. Catal. 39 (1975) 155.
[8] R. Carson, E.M. Cooke, J. Dwyer, A. Hinchliffe, P.J. O'Malley, Zeolites as Catalysts, Sorbants and Detergent Builders, Extended Abstracts (1988) 151.
[9] E. Kassab, K. Seiti, M. Allavena, J. Phys. Chem. 92 (1988) 6705.
[10] P.O. Fritz, J.H. Lunsford, J. Catal. 118 (1989) 85.
[11] A.G. Ashton, S. Batmanian, D.M. Clark, J. Dwyer, F.R. Fitch, A. Hinchcliffe, F.J. Mochado, in: B. Imelik, et al. (Eds.), Catalysis by Acids and Bases, in: Stud. Surf. Sci. Catal., vol. 20, Elsevier, Amsterdam, 1985, p. 101.
[12] R.M. Lago, W.O. Haag, R.J. Mikovsky, D.H. Olson, S.D. Hellring, K.D. Schmitt, G.T. Kerr, in: Y. Murakami, A. Iijima, J.W. Ward (Eds.), Proc. 7th Int. Zeol. Conference, Elsevier, Amsterdam, 1986, p. 677.
[13] Y. Sendoda, Y. Ono, Zeolites 8 (1988) 101.
[14] N.Y. Topsoe, F. Joensen, E.G. Derouane, J. Catal. 110 (1988) 404.
[15] E. Brunner, H. Ernst, D. Freude, M. Hunger, C.B. Krause, D. Prager, W. Reschetilowski, W. Schwieger, K.H. Bergk, Zeolites 9 (1989) 282.
[16] M.H. Vasques, F. Romoa Ribeiro, N.S. Gnep, M. Guisnet, React. Kinet. Catal. Lett. 38 (1989) 301.
[17] D.B. Lukyanov, Zeolites 11 (1991) 325.
[18] V.L. Zholobenko, L.M. Kustov, V.B. Kazansky, E. Loeffler, U. Lohse, C. Peuker, G. Oehlmann, Zeolites 10 (1990) 304.
[19] F. Lónyi, J.H.J. Lunsford, J. Catal. 136 (1992) 566.
[20] R. Carvajal, P.J. Chu, J.H. Lunsford, J. Catal. 125 (1990) 123.
[21] E.A. Lombardo, G.A. Sill, K.W. Hall, J. Catal. 119 (1989) 426.
[22] C. Miradatos, D. Barthomeuf, J. Chem. Soc., Chem. Commun. (1981) 39.
[23] A. Corma, J. Planelles, J. Sánchez-Marín, F. Thomás, J. Catal. 93 (1985) 30.
[24] W.O. Haag, R.M. Dessau, Proceedings of the 8th International Congress on Catalysis, vol. 2, Chemie, Weinheim, 1984, p. 305.
[25] K.A. Cumming, B.W. Wojciechowski, Catal. Rev.-Sci. Eng. 38 (1996) 101.
[26] W.O. Haag, R.M. Dessau, R.M. Lago, in: T. Inui, S.A. Namba, T. Tatsumi (Eds.), Chemistry of Microporous Materials, in: Stud. Surf. Sci. Catal., vol. 60, Elsevier, Amsterdam, 1991, p. 255.
[27] T.F. Narbeshuber, H. Vinek, J.A. Lercher, J. Catal. 157 (1995) 388.
[28] J.A. van Bokhoven, B.A. Williams, W. Ji, D.C. Koningsberger, H.H. Kung, J.T. Miller, J. Catal. 224 (2004) 50.
[29] W.O. Haag, in: J. Weitkamp, H.G. Karge, W. Hölderich (Eds.), Zeolites and Related Materials: State of the Art 1994, in: Stud. Surf. Sci. Catal., vol. 84, Elsevier Science B.V., Amsterdam, 1994, p. 1375.
[30] S.M. Babitz, B.A. Williams, J.T. Miller, R.Q. Snurr, W.O. Haag, H.H. Kung, Appl. Catal. A 179 (1999) 71.
[31] J.A. van Bokhoven, J.A.Z. Pieterse, M. Tromp, D.C. Koningsberger, J.T. Miller, J.A. Lercher, B.A. Williams, H.H. Kung, J. Catal. 202 (2001) 129.
[32] J.A. Lercher, A. Brait, K. Seshan, T.F. Narbeshuber, Appl. Catal. A 146 (1996) 119.
[33] T.F. Narbeshuber, Ph.D. thesis, University of Twente (1994) 51.
[34] G.C. Bond, M.A. Keane, J.A. Lercher, Catal. Rev.-Sci. Eng. 42 (2000) 323.
[35] J.F. Denayer, G.V. Baron, W. Souverijns, J.A. Martens, P.A. Jacobs, Ind. Eng. Chem. Res. 36 (8) (1997) 3242.
[36] F.J.M.M. de Gauw, J. van Grondelle, R.A. van Santen, J. Catal. 206 (2002) 295.
[37] M.A. Kuehne, H.H. Kung, J.T. Miller, J. Catal. 171 (1997) 293.
[38] Y. Hong, V. Gruver, J.J. Fripiat, J. Catal. 150 (1994) 421.
[39] C. Baerlocher, W.M. Meier, et al., Atlas of Zeolite Framework Types, fifth ed., Elsevier, Amsterdam, 2001.
[40] I.C. Arik, J.F. Denayer, G.V. Baron, Micropor. Mesopor. Mater. 60 (2003) 111.

[41] B.A. Williams, W. Ji, J.T. Miller, R.Q. Snurr, H.H. Kung, Appl. Catal. A 203 (2001) 179–190.
[42] F. Eder, M. Stockenhuber, J.A. Lercher, J. Phys. Chem. B 101 (1997) 5414.
[43] S. Kotrel, M.P. Rosynek, J.H. Lunsford, J. Phys. Chem. B 103 (1999) 818.
[44] B.A. Williams, S.M. Babitz, J.T. Miller, R.Q. Snurr, H.H. Kung, Appl. Catal. A 177 (1999) 161–177.